PHYSICAL REVIEW B VOLUME 3, NUMBER 8 15 APRIL 1971

Second-Harmonic Generation and Spin Decoupling in Resonant Two-Level Spin Systems

R. Boscaino, I. Ciccarello, C. Cusumano, and M. W. P. Strandberg*
Istituto di Fisica dell'Università, Palermo, Italy
and Gruppi Nazionali Strutture della Materia of the Consiglio Nazionale della Ricerche, Roma, Italy
(Received 20 August 1970)

A paramagnetic spin system is intrinsically nonlinear, and especially so at resonance; therefore, in the presence of a strong rf magnetic field it exhibits magnetic polarization at harmonic frequencies. We report here a complete set of experimental data on second-harmonic generation by a resonant *two-level* spin system. A theory is also developed, using the density-matrix formalism, which fully accounts for the experimental data. It is suggested that these harmonic signals are convenient to use for the measurement of the transverse relaxation time in saturated and unsaturated spin systems.

I. INTRODUCTION

Second-harmonic absorption has been widely investigated from the time the laser became available as a laboratory tool. A very intense beam of laser light creates a strong electromagnetic field. In intense electromagnetic (EM) fields, all dielectrics without a center-of-inversion symmetry are nonlinear; that is, the polarization is not linearly dependent on the electric field, but contains terms quadratic, cubic, etc., in the field amplitude. These higher-order terms give rise to harmonic waves in dielectrics interacting with a strong EM wave. Quantum mechanically, this process may be described as double (or multiple) quantum absorption through virtual states and relaxation to the fundamental state with the emission of harmonic frequencies.

The magnetic polarization of paramagnetic materials is similarly nonlinear in strong rf magnetic fields; harmonic generation is to be expected as an effect of double (or multiple) quantum transition. Furthermore, magnetic polarization increases very strongly at resonance. Resonance thus allows a relatively weak rf magnetic field to induce a magnetic polarization that is nonlinear at resonance, and harmonic effects are to be expected. In order to have a detectable second-harmonic signal, the driving rf magnetic field should be strong enough to bring the spin system to saturation at resonance. As we shall see, saturation plays an important role in the multiple quantum processes and harmonic generation. To be specific, one can think of a two-level spin system ($S = \frac{1}{2}$) in an external magnetic field H_0 with a relatively strong resonant rf field $H_{rf}(\omega)$ present at the same time. The effect of the rf field saturation is to produce broadening of the absorption line in first order[1,2] and at the same time to induce double (or multiple) quantum absorption and, as a consequence, to generate harmonic signals[3]; that is, the spin system operates as a frequency converter or heterodyne mixer, allowing rf power at the fundamental frequency to produce a polarization with frequencies $n\omega$, which produces emission at higher harmonic frequencies, and, when $n = 0$, to change the static polarization of the spin system.

A qualitatively different case would be one in which the splitting of the two-spin levels is twice the energy of the input photons. In this case, the spin system is not apparently saturated; still, as we shall see, it gives rise to second-harmonic emission.

Harmonic generation by spin systems has been discussed by Bloembergen and Shen.[4] Our theoretical development is implicit in their work, or, for that matter, in that of Karplus and Schwinger,[1] and that of Karplus.[2] Karplus and Schwinger[1] bring the calculation of nonlinear effects to the point where they must consider polarization of the system at harmonic frequencies, but they choose to drop these terms as being irrelevant to the effect of saturation which they wished to discuss. We carry out a calculation here that makes explicit the dependence of the harmonic emission on saturation effects. Since in experiments at microwave frequencies we can observe the effect of the vector polarization at the harmonic frequencies only by its projection on the observing (receiving) cavity mode, we have also made explicit and carefully studied the effect to be expected when that projection is varied. A further contribution that we make is to consider the effect of intense rf fields on the transverse relaxation parameter T_2.

Double quantum absorption by spin systems, on the other hand, has been studied especially at low fields[5-8] and calculated theoretically by many authors.[6,9-11] Often only the qualitative behavior is considered because of the difficulty of making exact calculations of the matrix elements involved.

In summary, we present here a complete set of experimental data on second-harmonic generation

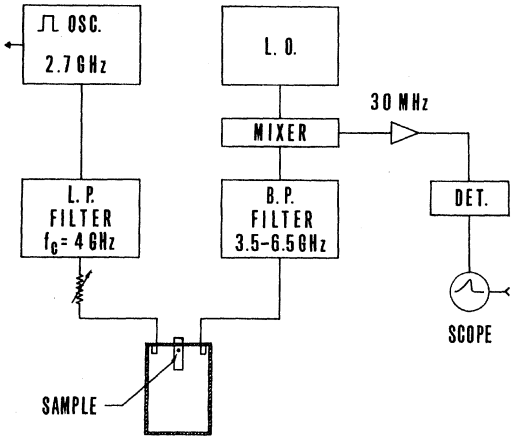

FIG. 1. Block diagram of the spectrometer used for second-harmonic generation in paramagnetic systems. Most of the experiments reported here were carried out at 2700→ 5400 MHz.

by a resonant two-level spin system. A theory is also developed, using the density-matrix formalism, which fully supports these experimental data.

II. EXPERIMENTAL APPARATUS AND RESULTS

The experimental apparatus used in the study of the second-harmonic generation is shown in Fig. 1. It is essentially the same as the one described previously,[3] except that a single double-mode cavity resonant at ω and 2ω is used, instead of two cavities coupled by a hole. The sample is located in a point of the cavity in which both the rf fields $H_{rf}(\omega)$ and $H_{rf}(2\omega)$ are maxima. Furthermore, the geometry of the cavity can be varied so that $H_{rf}(\omega)$ can be parallel or perpendicular to $H_{rf}(2\omega)$, and the external magnetic field H_0 can be rotated in a plane in which both $H_{rf}(\omega)$ and $H_{rf}(2\omega)$ lie.

The pulse oscillator is a triode oscillator giving a maximum peak power of the order of 1 kW, with a pulse length variable from 0.5 to 5 μsec, and with a repetition rate variable from 200 to 1000 pulses per sec. The low-pass filter reduces by more than 60 dB any harmonic content of the oscillator. Harmonic signals generated by the paramagnetic samples are filtered by a bandpass filter with 60-dB rejection at the fundamental. The signal is heterodyned to 30 MHz, amplified by a narrow-band amplifier (bandwidth approximately 1 MHz), detected, and displayed on the screen of a cathode-ray tube whose trace is synchronized with the pulse oscillator. The signal is seen in this way as a peak, the height of which is proportional to the harmonic signal amplitude.

For most of our experiments, the magnetic field geometry inside the bimodal cavity is the one shown in Fig. 2; $H_x(\omega)$ and $H_z(\omega)$ are therefore given by $H_{rf}(\omega)\cos\theta$ and $H_{rf}(\omega)\sin\theta$, respectively, and only the projections $M_x(2\omega)\cos\theta$ and $M_z(2\omega)\sin\theta$ of the components of the polarization $M_x(2\omega)$ and $M_z(2\omega)$ are detected.

Figure 3 shows the second-harmonic signal intensity vs external magnetic field H_0 for a specimen of dilute DPPH (sample No. 1) and Fig. 4 presents the harmonic spectrum of a sample of ruby ($Al_2O_3 + 0.1\%$ of Cr_2O_3) with the crystal c axis perpendicular to H_0. Two kinds of lines are present in both harmonic spectra. The ones with a more or less sharp "dip" at the center fall at those values of magnetic field at which two spin states of energy E_1 and E_2, respectively, are in resonance with the input rf power:

$$E_1 - E_2 = g\mu_B H_0 \equiv \hbar\omega_0 = \hbar\omega \ .$$

We shall call them $\omega \sim \omega_0$ lines. The bell-shaped lines correspond to the magnetic field such that

$$E_1 - E_2 = g\mu_B H_0 \equiv \hbar\omega_0 = 2\hbar\omega \ ;$$

we shall call them $\omega \sim \frac{1}{2}\omega_0$ lines.

The maxima of the $\omega \sim \omega_0$ line are 20 dB or more below the maximum of the $\omega \sim \frac{1}{2}\omega_0$ line. The ratio of the relative intensities depends, however, on the input rf power or, rather, on the saturation factor.

The peculiar shape of the $\omega \sim \omega_0$ line, with the sharp dip at resonance, was observed at 4.2 °K in all samples investigated, at least in the range of high input power levels. In particular, we observed that in ruby with 0.1% of Cr^{3+} concentration and in diluted DPPH (sample No. 1) the dip, more or less pronounced, is present over the full range of power available, while in a concentrated sample of DPPH (sample No. 2) the dip changes more drastically with the input power, and eventually, it disappears at low power levels as shown in Fig. 5. All of the data shown in Fig. 5 are taken at

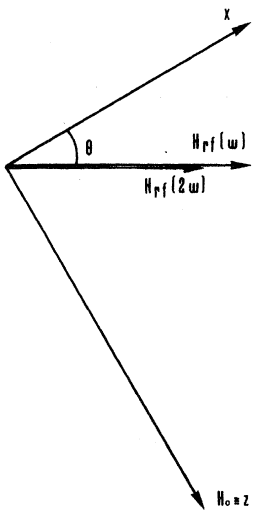

FIG. 2. Magnetic field geometry inside the bimodal cavity of Fig. 1, at the point where the sample is located. By rotating the external field H_0, the angle θ can be varied from 0° to 360°.

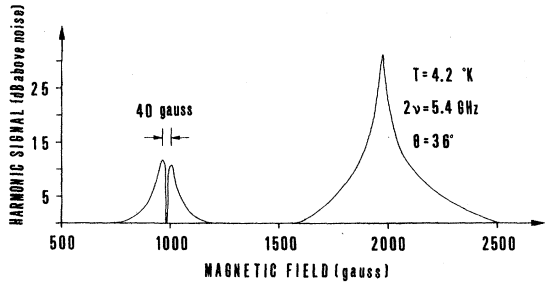

FIG. 3. Second-harmonic output power as a function of the external magnetic field in a sample of diluted DPPH, sample No. 1. Input peak power approximately 50 W. Measurements are taken point by point.

a fixed value of $\theta = 36°$. We wish to point out, however, that a variation of the angle θ has the same effect as a variation of the input power. Thus, with an input power of 50 W and $\theta = 36°$, the dip is not present in the $\omega \sim \omega_0$ line [Fig. 5(b)], but it appears if we operate at a smaller angle, that is, $\theta = 15°$. On the other hand, with an input power of 100 W, the dip of Fig. 5(c) disappears for angles greater than 36°, that is, $\theta = 70°$. This suggests that only the x component of the rf field, $H_{rf}\cos\omega t$, affects the line shape. We shall see from the theoretical expressions for the harmonic polarization that this angular dependence arises from the saturation factor $S = \gamma H_x (T_1/T_2)^{1/2}$.

For DPPH, sample No. 1, and for ruby with 0.1% of Cr^{3+} concentration, the linewidth as measured between the points of maximum signal is roughly independent of the input power over the full range of power investigated, while this is not true for the concentrated sample No. 2 of DPPH (see Fig. 5), though it should be so at very high input power levels.

For the power dependence, we found that the maximum of the $\omega \sim \frac{1}{2}\omega_0$ lines varies with the input power to the exponent 2 ± 0.1. This result is slightly in disagreement, but more accurate, than the result reported by Boscaino *et al.*[3] The quadratic dependence supports the hypothesis that two-photon absorption is responsible for the harmonic generation. For the $\omega \sim \omega_0$ lines, the power dependence measurements are less accurate because of the weaker signals, but we find that the harmonic signal varies approximately as $P^{1.7\pm0.2}$.

The temperature dependence of the harmonic signal has not been accurately measured, but it can be argued from Fig. 1 of Boscaino *et al.*[3] that the harmonic signal of both types of lines decreases with increasing temperature.

The harmonic signal vs θ (the angle defined in Fig. 2) at a given value of the magnetic field for the $\omega \sim \frac{1}{2}\omega_0$ line in ruby with 0.1% Cr^{3+} is shown in Fig. 6. It has a maximum for $\theta \sim 36°$, and it goes to zero at both $\theta = 0°$ and $\theta = 90°$. The experimental points are fitted quite well by the function $(\sin\theta\cos^2\theta)^2$, for both types of lines.

We should remark that the harmonic signal that we detect is a pulse that has roughly the same shape as that of the input pulse at the fundamental frequency, and there is no measurable delay time between the two pulses. Furthermore, the harmonic pulse is phase coherent. In order to check the phase coherence, we derived a second-harmonic signal from the pulse oscillator. This was sent through a variable phase shifter and variable attenuator, and finally mixed with the harmonic signal emitted by the sample. The two signals interfered destructively or constructively, depending on their relative phase difference. In this way, we could measure the phase variation of the harmonic signal while varying the external magnetic field H_0 through the resonance conditions. For the $\omega \sim \omega_0$ line of DPPH, sample No. 1, the phase variation is shown in Fig. 7(a), while Fig. 7(b) presents the phase variation for the $\omega \sim \frac{1}{2}\omega_0$ line. As a consequence of the phase coherence the har-

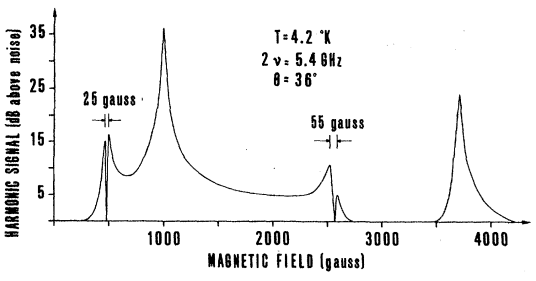

FIG. 4. Second-harmonic output power as a function of the external magnetic field in a ruby sample with 0.1% of Cr^{3+} concentration, crystal c axis perpendicular to H_0. Input peak power approximately 50 W. Measurements are taken point by point.

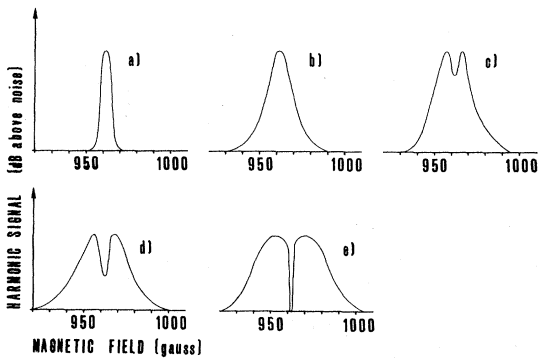

FIG. 5. Second-harmonic line near $\omega = \omega_0$ in a concentrated sample of DPPH, sample No. 2, at different input power levels. Frequency 2.7→5.4 GHz, $T = 4.2$ °K, $\theta = 36°$. Input peak powers: (a) ~5 W, (b) ~50 W, (c) ~100 W, (d) ~200 W, (e) ~400 W.

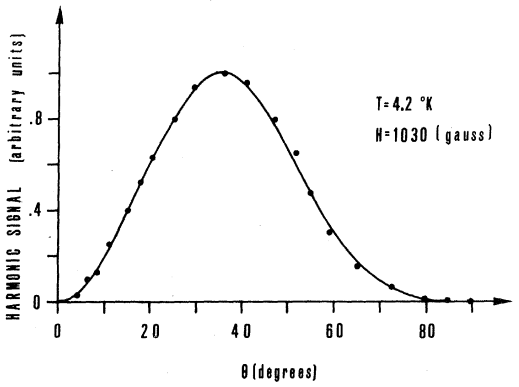

FIG. 6. Second-harmonic output power as a function of θ, the angle defined in Fig. 2, in a sample of ruby with 0.1% of Cr^{3+} concentration. Dots are experimental points, continuous line is a plot of the function $\sin^2\theta \times \cos^4\theta$; $\omega \sim \frac{1}{2}\omega_0$.

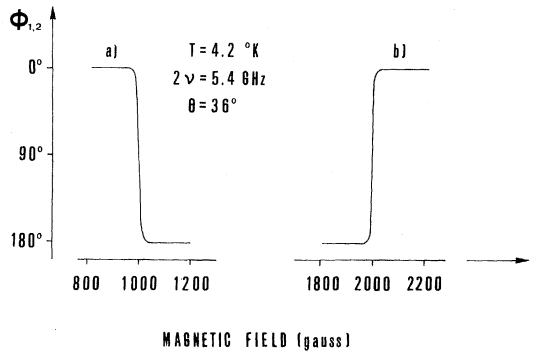

FIG. 7. Phase of the harmonic signal as a function of the external magnetic field in a sample of diluted DPPH (sample No. 1). Input peak power approximately 50 W.

monic signal also possesses energy or frequency coherence. No matter what the energy splitting of the spin states the "harmonic" signal contains only frequencies that are twice the fundamental carrier frequency plus the modulation sideband frequencies. We measured paramagnetic signals at frequencies $2\nu \pm \Delta\nu$, by changing the heterodyne oscillator frequency an amount $\Delta\nu$. The signal was observed to decrease very rapidly on increasing $\Delta\nu$ more than the bandwidth of the 30-MHz amplifier. Quantitative data are reported in Fig. 8.

III. THEORY

We consider a system of paramagnetic ions with effective spin $S = \frac{1}{2}$ in a static magnetic field $\vec{H}_0$, the direction of which fixes the z axis, and in an rf magnetic field $\vec{H}_{rf}\cos\omega t$ linearly polarized in a direction making an angle θ with the x axis. (See Fig. 2.) $\vec{H}_{rf}$ is assumed to be small but not negligible in comparison with $\vec{H}_0$, and therefore all terms involving the saturation factor are properly taken into account in our calculations. We call T_1 the longitudinal, and T_2 the transverse, relaxation time. As expected from Redfield's theory,[12,13] T_2 depends on the saturation of the spin system; consequently, we call T_{2o} and T_{2e} the transverse relaxation times, respectively, for a nonsaturated and a saturated spin system.

We make use of the density-matrix formalism,[1,4] and we define the density-matrix operator ρ in the usual way, averaged over an ensemble of identical systems. The average of any physical operator A is given by $\langle A\rangle = \mathrm{Tr}\rho A$, where Tr is the trace sum.

The equation of motion of the density matrix is given by

$$i\hbar\frac{\partial\rho}{\partial t} = \mathcal{H}\rho - \rho\mathcal{H} + i\hbar\left(\frac{\partial\rho}{\partial t}\right)_{\text{relax}}, \tag{1}$$

where $\mathcal{H}$ is the Hamiltonian of the generic spin

$$\mathcal{H} = \mathcal{H}_0 - \vec{\mu}\cdot\vec{H}_{rf}\cos\omega t = \mathcal{H}_0 + \mathcal{H}' . \tag{2}$$

$\mathcal{H}_0 = -\mu_z H_0$ is the time-independent Hamiltonian, and $\vec{\mu}$ is the magnetic moment operator.

By substituting (2) in (1) and separating the contribution that is due to $\mathcal{H}_0$ from that which is due to $-\vec{\mu}\cdot\vec{H}_{rf}\cos\omega t$, in the representation in which $\mathcal{H}_0$ is diagonal, we obtain

$$\left(\frac{\partial}{\partial t} + i\omega_{mn}\right)\rho_{mn}(t) = -\frac{i}{\hbar}\sum_k\left(\mathcal{H}'_{mk}\rho_{kn}(t) - \rho_{mk}(t)\mathcal{H}'_{kn}\right) - \frac{\rho_{mn}(t)-\rho^0_{mn}(t)}{T}, \tag{3}$$

where $T = T_1$ for $m = n$, $T = T_2$ for $m \neq n$, and $\rho^0_{mn}(t)$ is the matrix element of the operator defined by

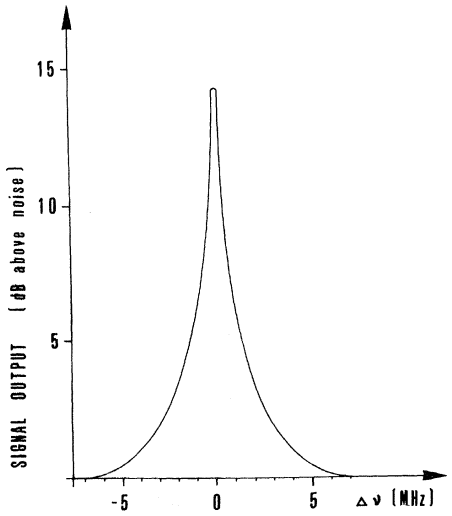

FIG. 8. Frequency spectrum of the "harmonic" signal for sample No. 1 of DPPH. $\Delta\nu = 0$ corresponds to the exact harmonic frequency $2\nu = 5.4$ GHz.

$$\rho^0(t)=e^{-\mathcal{H}/kT}/\mathrm{Tr}e^{-\mathcal{H}/kT}\ .$$

We look for the steady-state solution of Eq. (3) which we write in a Fourier expansion in ω:

$$\rho_{mn}(t)=\rho_{mn}(dc)+\rho^{\pm}_{mn}(\omega)\,e^{\mp i\omega t}+\rho^{\pm}(2\omega)\,e^{\mp 2i\omega t}+\cdots\ , \tag{4}$$

where $\rho_{mn}(dc)$ is different from the thermal equilibrium value

$$\rho^0_{mn}=\frac{\exp[(-\mathcal{H}_0)_{mn}/kT]\delta_{mn}}{\mathrm{Tr}\exp(-\mathcal{H}_0/kT)}\ ,$$

since it includes the static contributions attributable to the time-dependent Hamiltonian.

The solution of the equation of motion (3) is obtained in two steps. First, following the procedure of Karplus and Schwinger,[1] we calculate the coefficients $\rho^{\pm}_{mn}(\omega)$ in the approximation in which all contributions from terms varying at harmonic frequencies in (4) are neglected. We then use $\rho^{\pm}_{mn}(\omega)$ in order to calculate the coefficients $\rho^{\pm}_{mn}(2\omega)$. By substituting Eq. (4), without the harmonic terms, in Eq. (3) we get for $\rho^{\pm}_{mn}(\omega)$ the following expression[1]:

$$[\rho^{-}_{nm}(\omega)]^x=\rho^{+}_{mn}(\omega)$$

$$=\frac{\omega\mu_{mnx}H_x(\rho^0_{mm}-\rho^0_{nn})[(\omega-\omega_{mn})-i/T_2]}{2\hbar\omega_{mn}[(\omega-\omega_{mn})^2+1/T_2^2+S^2]}\ , \tag{5}$$

where the saturation factor S stands for $S=\gamma H_x\times(T_1/T_2)^{1/2}$. We have dropped from Eq. (5) terms containing $H_z(\omega)$, since they give a negligible contribution for $\omega T_1\gg 1$. This condition will always be satisfied in our experiments.

From Eq. (3) we can derive the equation of motion for terms varying at 2ω:

$$(-2i\omega+i\omega_{mn}+1/T)\,\rho^{+}_{mn}(2\omega)$$

$$=-(i/2\hbar)\sum_k(\mathcal{H}'_{mk}\rho^{+}_{kn}(\omega)-\rho^{+}_{mk}(\omega)\mathcal{H}'_{kn})\ . \tag{6}$$

We solve Eq. (6) by considering separately the effects of the off-diagonal and diagonal perturbations on the 2ω terms. For the off-diagonal perturbation the matrix elements $\mathcal{H}'_{mk}$ in Eq. (6) are given by

$$\mathcal{H}'_{mk}=-\mu_{mkx}H_x\cos\omega t\ . \tag{7}$$

By substituting (7) in (6) for a two-level spin system, we obtain

$$\rho^{+}_{mm}(2\omega)=-\rho^{+}_{nn}(2\omega)=\frac{i[\mu_{mnx}\rho^{+}_{nm}(\omega)-\rho^{+}_{mn}(\omega)\mu_{nmx}]H_x}{2\hbar(-2i\omega+1/T_1)}\ ,$$

and using (5) with $\omega_0=\omega_{mn}$, we have

$$\rho^{+}_{mm}(2\omega)=\frac{i\omega|\mu_{mnx}|^2H_x^2(\rho^0_{mm}-\rho^0_{nn})}{4\hbar^2\omega_0(-2i\omega+1/T_1)}$$

$$\times\left(\frac{(\omega_0-\omega)-i/T_2}{(\omega-\omega_0)^2+1/T_2^2+S^2}-\frac{(\omega+\omega_0)-i/T_2}{(\omega+\omega_0)^2+1/T_2^2+S^2}\right)\ . \tag{8}$$

The expectation value of $M_z(2\omega)$ is

$$M_z(2\omega)=2\,\mathrm{Re}\sum_m\mu_{mmz}\rho^{+}_{mm}(2\omega)\,e^{-2i\omega t}$$

$$=4\,\mathrm{Re}[\mu_{mmz}\rho^{+}_{mm}(2\omega)\,e^{-2i\omega t}]\ ,$$

since for a two-level spin system $\mu_{mmz}=-\mu_{nnz}$. By substituting Eq. (8) in the last expression and retaining only the resonant terms, near $\omega=\omega_0$, we have

$$[M_z(2\omega)]_{\omega\sim\omega_0}=\frac{\mu_{mmz}|\mu_{mnx}|^2H_x^2(\rho^0_{mm}-\rho^0_{nn})}{2\hbar^2\omega_0}$$

$$\times\frac{(\omega-\omega_0)\cos2\omega t-(1/T_{2e})\sin2\omega t}{(\omega-\omega_0)^2+1/T_{2e}^2+S^2}\ . \tag{9}$$

For a diagonal perturbation the matrix elements in the equation of motion (6) are

$$\mathcal{H}'_{mk}=-\mu_{mmz}H_z\cos\omega t\,\delta_{mk}\ .$$

For a two-level spin system, using Eq. (5), we find the following solutions:

$$\rho^{+}_{mn}(2\omega)=\frac{i\omega\mu_{mmz}H_z\mu_{mnx}H_x(\rho^0_{mm}-\rho^0_{nn})}{2\omega_0\hbar^2(-2i\omega+i\omega_0+1/T_2)}$$

$$\times\frac{(\omega-\omega_0)-i/T_2}{[(\omega-\omega_0)^2+1/T_2^2+S^2]}=[\rho^{-}_{nm}(2\omega)]^*\ . \tag{10}$$

Proceeding in a similar way, used to compute $M_z(2\omega)$, and neglecting trivial nonresonant terms, we obtain for $M_x(2\omega)$

$$M_x(2\omega)=2\,\mathrm{Re}\left(\frac{i\omega\mu_{mmz}|\mu_{mnx}|^2H_xH_z(\rho^0_{mm}-\rho^0_{nn})}{2\hbar^2\omega_0(-2i\omega+i\omega_0+1/T_2)}\right.$$

$$\left.\times\frac{[(\omega-\omega_0)-i/T_2]}{[(\omega-\omega_0)^2+1/T_2^2+S^2]}\,e^{-2i\omega t}\right). \tag{11}$$

There will be an identical expression for $M_y(2\omega)$, but with a time phase shifted by i. In the following discussion we shall ignore this component of $\vec{\mathbf{M}}(2\omega)$ because it is not observed in our experiments. This is proper because the coordinate axes perpendicular to the static field are arbitrarily defined in any case. The observation of any component of $\vec{\mathbf{M}}(2\omega)$ in the x-y plane thus determines all components in that plane.

$M_x(2\omega)$ given by (11) has two resonances, one at $\omega=\omega_0$ and one at $\omega=\frac{1}{2}\omega_0$. $M_x(2\omega)$ near $\omega=\omega_0$ may be written

$$[M_x(2\omega)]_{\omega\sim\omega_0}=-\frac{\mu_{mmz}|\mu_{mnx}|^2H_xH_z(\rho^0_{mm}-\rho^0_{nn})}{\omega_0\hbar^2}$$

$$\times\frac{(\omega-\omega_0)\cos2\omega t-(1/T_{2e})\sin2\omega t}{[(\omega-\omega_0)^2+1/T_{2e}^2+S^2]}\ , \tag{12}$$

while near $\omega = \frac{1}{2}\omega_0$,

$$[M_x(2\omega)]_{\omega\sim\omega_0/2} = \frac{\mu_{mmz}|\mu_{mnx}|^2 H_x H_z(\rho^0_{mm}-\rho^0_{nn})}{\hbar^2\omega_0} \times \frac{(2\omega-\omega_0)\cos 2\omega t - (1/T_{2o})\sin 2\omega t}{[(2\omega-\omega_0)^2+1/T_{2o}^2]} . \quad (13)$$

We have called T_{2o} the transverse relaxation time in Eq. (13) and T_{2e} the transverse relaxation time in Eqs. (9) and (12). The two values T_{2o} and T_{2e} are expected to be different.[12,13] T_{2e} is the relaxation time measured with saturation of the spin system. In Eq. (13), however, T_{2o} is the relaxation time measured at approximate thermal equilibrium, since the spin system for this case is not resonant with the input power.

In summary, we have solved the equation of motion of the density matrix for a two-level spin system for terms varying at the second-harmonic frequency. The solution shows that a perturbing rf field $H_x(\omega)$ gives rise to a magnetization $M_z(2\omega)$ that is resonant at $\omega=\omega_0$, while the simultaneous presence of both $H_x(\omega)$ and $H_z(\omega)$ gives rise, in addition to $M_z(2\omega)$, to a magnetization $M_x(2\omega)$ that is resonant at $\omega=\omega_0$ and $\omega=\frac{1}{2}\omega_0$.

These components of the magnetization, $M_x(2\omega)$ and $M_z(2\omega)$, are magnetic dipoles that irradiate power at frequency 2ω proportional to $|M_x(2\omega)|^2$ and $|M_z(2\omega)|^2$. The magnetization, and therefore the spin system, through this mechanism converts power from the fundamental to harmonic frequencies, increasing the entropy of the system.

The conversion of power from the fundamental to the second-harmonic frequency by a resonant two-level spin system can be described in terms of Raman-like processes induced by photons.[4] In particular, in the case of lines resonating at $\omega=\omega_0$, one spin in the excited state can absorb a photon and decay to the fundamental state with the emission of one photon of harmonic frequency. A different process can be the one in which the spin in the ground state absorbs two photons going to a virtual level from which it relaxes to the ground state with the emission of one harmonic photon. Other processes are also possible. A more detailed discussion of these processes is given by Persico and Vetri.[14] We want to point out here that processes in which the spin does not change state are probably the ones responsible for the observed harmonic emission; this is because they are expected to have a quadratic power dependence and phase coherence of the harmonic signal.

IV. DISCUSSION

In order to make a comparison between the theory and experimental data, we refer to the magnetic field geometry of Fig. 2, which is the one used in most of our experiments. In this case, $H_x(\omega) = H_{rf}(\omega)\cos\theta$ and $H_z(\omega) = H_{rf}(\omega)\sin\theta$. Because $H_{rf}(2\omega)$ is parallel to $H_{rf}(\omega)$, the power emitted into the 2ω mode of the cavity is proportional to

$$[M_x(2\omega)\cos\theta + M_z(2\omega)\sin\theta]^2 ,$$

where $M_x(2\omega)$ and $M_z(2\omega)$ are given by Eqs. (12), (13), and (9). Near $\omega=\frac{1}{2}\omega_0$ only $M_x(2\omega)$ is important, and the harmonic signal is proportional to the amplitude of

$$P^{(2\omega)}_{\omega\sim\omega_0/2} \propto \left[\frac{H^2_{rf}\cos^2\theta\sin\theta(\rho^0_{mm}-p^0_{nn})}{\omega_0}\right]^2 \times \frac{\cos^2(2\omega t+\phi)}{[(2\omega-\omega_0)^2+1/T^2_{2o}]} , \quad (14)$$

where ϕ is given by

$$\tan\phi = \frac{1/T_{2o}}{2\omega-\omega_0} . \quad (15)$$

Equation (14) accounts quite well for the bell-shaped lines at $\omega\sim\frac{1}{2}\omega_0$ of Figs. 3 and 4. It shows the quadratic power dependence as observed experimentally and the correct angular dependence $(\cos^2\theta \times \sin\theta)^2$ (see Fig. 6).

Even the temperature dependence, essentially given by the factor $(\rho^0_{mm}-\rho^0_{nn})^2$, is in qualitative agreement with the approximate temperature dependence, which can be inferred from Fig. 1 of Ref. 3.

The good agreement of the theory with the experimental results is a persuasive argument for the correctness of Eq. (14), in spite of the approximations used, and it suggests the use of Eq. (15) to measure the spin-spin relaxation time T_{2o} for the unsaturated condition by measurement of the relative phase of the second-harmonic signal. We have made measurements of the phase of the harmonic signal near the $\omega=\frac{1}{2}\omega_0$ resonance, in the manner described in Sec. II, and using Eq. (15), we find for the sample No. 1 of DPPH at 4.2 °K that $T_{2o}=5.5\times10^{-9}$ sec; for a sample of ruby with 0.1% of Cr^{3+} concentration at the same temperature, we find $T_{2o}=3.5\times10^{-9}$ sec.

The harmonic signal near $\omega=\omega_0$ arises both from $M_x(2\omega)$ of Eq. (12) and $M_z(2\omega)$ of Eq. (9); therefore, it is proportional to the amplitude of

$$P^{(2\omega)}_{\omega\sim\omega_0} \propto \left[\frac{H^2_{rf}\sin\theta\cos^2\theta(\rho^0_{mm}-\rho^0_{nn})}{2\omega_0}\right]^2 \times \frac{(\omega-\omega_0)^2+1/T^2_{2e}}{[(\omega-\omega_0)^2+1/T^2_{2e}+S^2]^2}\cos^2(2\omega t+\phi_1) , \quad (16)$$

where ϕ_1 is given by

$$\tan\phi_1 = \frac{1/T_{2e}}{\omega-\omega_0} . \quad (17)$$

Equation (16) accounts quite well for the experimental line shapes of the $\omega\sim\omega_0$ lines of Figs. 3 and 4.

The harmonic signal near $\omega=\omega_0$ described by Eq. (16) for $S\gg 1/T_{2e}$ (high input power) will show a line shape with a pronounced "dip" at the center and two maxima at $(\omega-\omega_0)^2\cong S^2-1/T_{2e}^2$; while for $S\ll 1/T_{2e}$ (low input power) Eq. (16) describes a bell-shaped line with a maximum at $\omega=\omega_0$. This behavior was observed, as reported in Sec. III, in our samples of DPPH and ruby. In particular, we believe that the condition $ST_{2e}<1$ is never reached for the diluted sample No. 1 of DPPH, even at the lowest input power, because of the long spin-lattice relaxation time,[15] and therefore the dip is expected to be present in the full range of power investigated. For the concentrated sample No. 2 of DPPH the condition $ST_{2e}=1$ is reached when the input peak power is of the order of 50 W, as can be inferred from Fig. 5. Finally, for ruby with 0.1% of Cr^{3+} concentration the dip is observed experimentally at all power levels. This can be due to the fact that the condition $ST_{2e}<1$ is never reached, as for sample No. 1 of DPPH. The fact that Eq. (16), when applied to ruby, should be modified in order to properly take into account the inhomogeneous broadening of the line[16] is probably not relevant, since this modification would affect both the $\omega=\omega_0$ line and the $\omega=\frac{1}{2}\omega_0$ line; but the $\frac{1}{2}\omega_0$ line appears to be normal.

For $S\gg 1/T_{2e}$ the second-harmonic signal amplitude at $(\omega-\omega_0)^2=S^2-1/T_{2e}^2$ is proportional to

$$P_{\max}^{(2\omega)}\propto (H_{rf}^2\cos^2\theta\sin\theta)^2/S^2 \quad . \tag{18}$$

Since

$$S^2=\gamma^2 H_{rf}^2\cos^2\theta\, T_1/T_{2e},$$

we would expect $P_{\max}^{(2\omega)}$ of Eq. (18) to vary linearly with the input rf power, and as $(\cos^2\theta\sin^2\theta)$ with the angle θ; this is actually in disagreement with the experimental results that show that

$$P_{\max}^{(2\omega)}\propto (H_{rf}^2)^{1.7}\,(\cos^2\theta\sin\theta)^2 \quad .$$

We should remark, however, that the previous discussion is valid only if T_1 and T_{2e} are independent of the input rf power. In particular, the spin-transition probability from a state of $S=\pm\frac{1}{2}$ to a state of $S=\mp\frac{1}{2}$ will increase proportional to the input power, or proportional to $H_{rf}^2(\omega)$. The magnetic field as seen at its neighbors will thus tend to average to zero as the input power increases. T_{2e} is thus expected to increase with the input power until it finally reaches a limiting value determined by the spin-lattice interaction, T_1.[12,13] We have therefore used Eq. (17) to determine the experimental values of T_{2e} at different input power levels in a manner similar to the method used to determine T_{2o}. Detailed data of T_{2e} vs input power will be published elsewhere.[17] We wish to point out here that our experimental data for the sample No. 1 of diluted DPPH at 4.2 °K show that T_{2e} is linearly dependent on H_x^2, that is, on the input power.[17] For the experimental conditions of Fig. 3 the value of T_{2e} that we obtained for sample No. 1 of DPPH from phase measurements was $T_{2e}=9\times10^{-8}$ sec, approximately 16 times T_{2o}. If we write $T_{2e}=T_{2o}+\alpha H_x^2$, then if we neglect the eventual power dependence of T_1, at high input power levels, $T_{2o}\ll\alpha H_x^2$, then the saturation term is expected to be constant times a term varying slowly with power:

$$S=\text{const}\,(1+T_{2o}/\alpha H_x^2)^{-1/2} \quad . \tag{19}$$

Putting (19) into (18), we obtain for $P_{\max}^{(2\omega)}$ an angular and input power dependence, in satisfactory agreement with experiment. The exponent of the power dependence is predicted to be $2-2T_{2o}/\alpha H_x^2\sim 1.8$, while the observed exponent is 1.7 ± 0.2. The angular dependence is predicted to be

$$[\sin\theta\cos^2\theta]^2$$

$$\times\left[1+\frac{1}{1+\gamma H_{rf}^2\cos^2\theta\; T_1\,T_{2o}(1+\alpha H_{rf}^2\cos^2\theta/T_{2o})}\right]^2 .$$

For a saturated spin system $\theta<\frac{1}{2}\pi$, this function differs trivially from the observed $(\sin\theta\cos^2\theta)^2$, while for $\theta\to\frac{1}{2}\pi$ the vanishing emission signal is merely doubled.

The linewidth of the $\omega\sim\omega_0$ line, defined as the frequency difference between points of maximum signal, is $\Delta\omega\sim 2S$, and, by virtue of (19), it is expected to be approximately independent of the input power at high power levels.

The ratio of the maximum of the $\omega\sim\frac{1}{2}\omega_0$ line to the maximum of the $\omega\sim\omega_0$ line is given by

$$\frac{A}{B}=\frac{P^{(2\omega)}_{\omega=\omega_0/2}}{P^{(2\omega)}_{(\omega-\omega_0)^2=S^2-1/T_{2e}^2}}\approx 16\,S^2\,T_{2o}^2 \quad . \tag{20}$$

Finally, the ratio of the maximum signal of the $\omega\sim\omega_0$ line to the minimum signal at $\omega=\omega_0$ of the same line is

$$\frac{B}{C}=\frac{P^{(2\omega)}_{(\omega-\omega_0)^2=S^2-1/T_{2e}^2}}{P^{(2\omega)}_{\omega=\omega_0}}\approx\frac{1}{4}\left(\frac{1}{T_{2e}S}+ST_{2e}\right)^2 \quad . \tag{21}$$

We shall now make a quantitative comparison with the experimental data that we have for sample No. 1 of diluted DPPH at 4.2 °K. As expected, the measured distance between the two maxima of the $\omega\sim\omega_0$ line is approximately constant and, in magnetic field units, is $\Delta H\approx 40$ G. This corresponds to a saturation factor $S=3.6\times10^6\ \text{sec}^{-1}$. By substituting this value of S in Eq. (20) and the value $T_{2o}=5.5\times10^{-9}$ sec derived from phase measurements, we get

$$\frac{A}{B}=16\,T_{2o}^2S^2\approx 60\to 18\ \text{dB} \quad ,$$

in good agreement with the experimental value of

A/B that can be deduced from Fig. 3. By substituting S and $T_{2e}=9\times10^{-8}$ sec in Eq. (21) we have, however,

$$B/C \approx \tfrac{1}{4} T_{2e}^2 S^2 \approx 250 \rightarrow 24 \text{ dB} \quad ,$$

which is greater than the value that can be read from Fig. 3; however, because the harmonic signal at $\omega=\omega_0$ has the same intensity as the noise, the true ratio B/C in Fig. 3 can be much greater than 13 dB. On the other hand, by substituting in the equation $S=\gamma H_x (T_1/T_2)^{1/2}$ the proper values of H_x, T_1, and T_2, we obtain for S, values very close to those obtained from linewidth measurements of the $\omega\sim\omega_0$ line.

Finally, we remark that all of the previous data are taken with the magnetic field geometry of Fig. 2. By using a different magnetic field geometry, we can split the second-harmonic emission signal into a contribution that is due to $M_x(2\omega)$ and one that is due to $M_z(2\omega)$. In particular, if we operate with $\vec{H}_{rf}(\omega)$ perpendicular to $\vec{H}_0$ and $\vec{H}_{rf}(2\omega)$ parallel to $\vec{H}_0$, only the component $M_z(2\omega)$ is different from zero, and, therefore, one single line, near $\omega=\omega_0$, is expected. Actually, by using a cavity with this magnetic field geometry, the detected harmonic spectrum shows only the $\omega\sim\omega_0$ line.

ACKNOWLEDGMENTS

We acknowledge very useful conversations with G. Vetri and F. S. Persico.

*On sabbatical leave from the Department of Physics and Research Laboratory of Electronics, Massachusetts Institute of Technology, Cambridge, Mass. 02139.

[1]R. Karplus and J. Schwinger, Phys. Rev. 73, 1020 (1948); M. A. Garstens and J. I. Kaplan, *ibid.* 99, 459 (1955).

[2]R. Karplus, Phys. Rev. 73, 1027 (1948).

[3]R. Boscaino, I. Ciccarello, and C. Cusumano, Phys. Rev. Letters 20, 421 (1968).

[4]N. Bloembergen and Y. R. Shen, Phys. Rev. 133, A37 (1964); N. Bloembergen, *Nonlinear Optics* (Benjamin, New York, 1965).

[5]J. Brossel, B. Cagnac, and A. Kastler, Compt. Rend. 237, 984 (1953).

[6]J. M. Winter, J. Phys. Radium 19, 802 (1958).

[7]G. Alzetta, E. Arimondo, C. Ascoli, and A. Gozzini, Nuovo Cimento 52B, 392 (1967).

[8]G. Alzetta, E. Arimondo, and C. Ascoli, Nuovo Cimento 54B, 107 (1968).

[9]J. M. Winter, Ann. Phys. (Paris) 4, 745 (1959).

[10]F. Lurcat, Arch. Sci. (Geneva) 11, 295 (1958).

[11]S. Wilking, Z. Physik, 173, 490 (1963).

[12]A. G. Redfield, Phys. Rev. 98, 1787 (1955).

[13]B. N. Provotorov, Zh. Eksperim. i Teor. Fiz. 41, 1582 (1961) [Soviet Phys. JETP 14, 1126 (1962)]; G. R. Khutsishvili, *ibid.* 50, 1641 (1966) [*ibid.* 23, 1092 (1966)].

[14]F. S. Persico and G. Vetri, Solid State Commun. 8, 1509 (1970).

[15]J. P. Goldsborough, N. Mandel, and G. E. Pake, Phys. Rev. Letters 4, 13 (1960).

[16]W. J. C. Grant and M. W. P. Strandberg, Phys. Rev. 135, A727 (1964).

[17]R. Boscaino, I. Ciccarello, and M. W. P. Strandberg (unpublished).

PHYSICAL REVIEW B VOLUME 3, NUMBER 8 15 APRIL 1971

Scattering from the E_1 Polariton of $LiIO_3$

C. K. Asawa and M. K. Barnoski

Hughes Research Laboratories, Malibu, California 90265

(Received 16 November 1970)

Raman scattering from an E_1 mode polariton of $LiIO_3$ is reported. A polariton with energy between 687 and 766 cm^{-1} is observed in near-forward scattering with $y(zx)\bar{y}$ polarization. The polariton is observed only near 764 cm^{-1} in the $y(xz)\bar{y}$ spectra. The results are analyzed. It is also found that the polariton dispersion curve does not change with the orientation of the phonon wave vector.

INTRODUCTION

It was shown by Huang[1] that transverse optical phonons of ionic crystals and photons with nearly the same wave vector and energy can be strongly coupled. The resulting mixed phonon-photon states are now referred to as "polaritons." Raman scattering from the polaritons of GaP was reported for the first time by Henry and Hopfield.[2] Shortly thereafter polariton scattering from anisotropic ZnO was reported by Porto *et al.*[3]

The Raman and polariton spectra of $LiIO_3$ have been examined recently by Claus *et al.*[4] These authors stated that *no* E_1 polariton was "unambiguously" observed [although an A polariton was observed in $x(yy)x$ polarization]. We wish to report the observation of an E_1 polariton in forward scattering in $LiIO_3$ and to clarify possible difficulties in the analysis of the experiments.

$LiIO_3$ belongs to the $P6_3(C_6^6)$ space group.[5] Twen-